



**University of Dundee**

## **Application of Three-dimensional IGN-2 Equations to Wave Diffraction Problems**

Zhao, Binbin ; Zhang, Tianyu ; Duan, Wenyang ; Ertekin, R. Cengiz; Hayatdavoodi, Masoud

*Published in:*  
Journal of Ocean Engineering and Marine Energy

*DOI:*  
[10.1007/s40722-019-00157-4](https://doi.org/10.1007/s40722-019-00157-4)

*Publication date:*  
2019

*Document Version*  
Peer reviewed version

[Link to publication in Discovery Research Portal](#)

*Citation for published version (APA):*  
Zhao, B., Zhang, T., Duan, W., Ertekin, R. C., & Hayatdavoodi, M. (2019). Application of Three-dimensional IGN-2 Equations to Wave Diffraction Problems. *Journal of Ocean Engineering and Marine Energy*.  
<https://doi.org/10.1007/s40722-019-00157-4>

### **General rights**

Copyright and moral rights for the publications made accessible in Discovery Research Portal are retained by the authors and/or other copyright owners and it is a condition of accessing publications that users recognise and abide by the legal requirements associated with these rights.

### **Take down policy**

If you believe that this document breaches copyright please contact us providing details, and we will remove access to the work immediately and investigate your claim.

This is a post-peer-review, pre-copyedit version of an article published in Journal of Ocean Engineering and Marine Energy. The final authenticated version is available online at: [http://dx.doi.org/\[insert DOI\]](http://dx.doi.org/[insert DOI])”.

# Application of Three-dimensional IGN-2 Equations to Wave Diffraction Problems

Binbin Zhao<sup>a</sup>, Tianyu Zhang<sup>a</sup>, Wenyang Duan<sup>a,\*</sup>, R. Cengiz Ertekin<sup>b,a</sup>, Masoud Hayatdavoodi<sup>c,a</sup>

<sup>a</sup>College of Shipbuilding Engineering, Harbin Engineering University, 150001 Harbin, China

<sup>b</sup>Department of Ocean & Resources Engineering, University of Hawai'i, Honolulu, HI 96822, USA

<sup>c</sup>School of Science and Engineering, University of Dundee, Dundee DD1 4HN, UK

---

## Abstract

We use the Level II Irrotational Green-Naghdi (IGN-2) equations to study a number of wave diffraction problems. The IGN-2 equations can model strongly nonlinear waves. The three-dimensional solution of the IGN-2 equations is developed in this work and applied to some three-dimensional wave transformation and diffraction problems. Three test cases are considered. First one is on wave evolution in a closed basin. It is shown that the IGN-2 results agree well with the linear analytical results for small wave amplitudes. The following two cases involve wave diffraction problems caused by an uneven seabed. In both of these cases, excellent agreement is obtained between the IGN-2 model and the experimental measurements and numerical predictions of others. It is concluded that IGN-2 model can be used to accurately model diffraction and transformation of nonlinear waves in three dimensions.

*Key words:* Irrotational Green-Naghdi theory, IGN-2 equations, wave evolution, wave transformation, wave diffraction

---

## 1. Introduction

The Green-Naghdi (hereafter, GN) theory was first introduced about forty years ago (Green et al., 1974; Green and Naghdi, 1976). To derive the GN equations, a shape-function that approximates the vertical distribution of the velocity field along the water column is

---

\*Corresponding author.

5 used. This is not the only way the GN equations can be derived, see, for example, the  
6 introduction sections of Kim et al. (2001) and Ertekin et al. (2014) for a discussion on the  
7 subject. In derivation of the GN equations, no other assumptions and approximations are  
8 introduced and no restriction is enforced on the rotationality of the flow field.

9 The GN theory is categorized into different levels, based on the approximation functions  
10 used to describe the distribution of the vertical velocity component along the water col-  
11 umn. For example, Ertekin et al. (1986) utilized the Level I equations to simulate waves  
12 generated by ships in restricted waters. Demirbilek and Webster (1992) applied the Level  
13 II model to some two-dimensional wave propagation problems. The higher level GN wave  
14 equations have been developed and it is shown that they provide accurate results for strongly  
15 nonlinear and strongly dispersive waves (Zhao et al., 2014). The GN-1 equations were also  
16 used in three-dimensional problems, see Neill and Ertekin (1997), Ertekin and Sundararagha-  
17 van (2003), Hayatdavoodi et al. (2018), Neill et al. (2018). Zhao et al. (2015a) developed  
18 the three-dimensional solution method for the high-level GN equations. We note here that  
19 three-dimensionality refers to the physical problem, and not to the theory or the equations  
20 themselves, as the vertical structure of the flow field in the theory is known a priori.

21 Although irrotationality of the flow field is not a requirement in general in deriving the  
22 GN equation, it is possible to obtain the equations for an irrotational flow. Kim et al. (2001)  
23 derived the Irrotational Green-Naghdi (IGN) equations from Hamilton's principle. The IGN  
24 equations for finite water depth were numerically tested to show their self-convergence and  
25 accuracy in two dimensions (Kim et al., 2003, 2010). Polynomial expansions are used to  
26 prescribe the velocity field in vertical distribution. In the IGN models, only the odd terms of  
27 the polynomial are used. Zhao et al. (2015b) showed that the two-dimensional IGN equations  
28 are more efficient to solve than the GN equations where the rotationality of the flow is weak.  
29 However, the three-dimensional IGN equations have not been studied so far. Zhao et al.  
30 (2016) studied the IGN-2 equations and showed that IGN-2 equations are strongly nonlinear  
31 equations. The IGN-2 equations give errors of less than 2% in calculation of the phase  
32 velocity from shallow-water depths up to  $kd = 4.87$ , where  $k$  is the wave number and  $d$  is

33 the water depth. Higher level GN and IGN equations are strongly nonlinear and strongly  
 34 dispersive wave equations.

35 The main motivation for this research is, therefore, to introduce the numerical model for  
 36 three-dimensional IGN-2 equations and apply it to some water-wave diffraction problems.  
 37 The intent of this paper is not to include very large waves and all the ranges of  $kd$ . In Section  
 38 2, the IGN equations are introduced. Section 3 presents the algorithm used in solving the  
 39 IGN-2 equations. The solution of the linearised IGN-2 equations is given in Section 4. Some  
 40 test cases simulated by the three-dimensional IGN-2 equations are presented in Section 5.  
 41 These are followed by our conclusions in Section 6.

## 42 2. IGN equations

43 In this work, three-dimensional wave problems are considered.  $x$  and  $y$  are the horizontal  
 44 coordinates, with  $x$  pointing to the right and  $y$  is into the paper, and  $z$  is the vertical  
 45 coordinate, positive up. The origin of the right-handed coordinate system is located at  
 46 the still-water level. The bottom boundary varies spatially,  $z = -h(x, y)$ . The free surface is  
 47 specified by  $z = \eta(x, y, t)$ . The pressure on the free surface is taken as zero, i.e.,  $\hat{p}(x, y, t) = 0$ ,  
 48 without loss in generality. The IGN equations used in this work are similar to those given  
 49 by Ertekin et al. (2014) who presented the two-dimensional IGN equations.

In three dimensions, the velocity field  $(u, v, w)$  that satisfies the kinematic constraints  
 are given by the stream function  $\Psi(x, y, z, t) = (\psi^u, \psi^v)$ , where  $(u, v)$  are the horizontal  
 components of velocity in the  $x$  and  $y$  direction, respectively, and  $w$  is the vertical component  
 in the  $z$  direction. Therefore

$$(u, v) = \Psi_{,z}, \tag{1a}$$

$$w = -\nabla \cdot \Psi, \tag{1b}$$

50 Where  $\nabla$  is the gradient operator. Here, we make  $\Psi(x, y, z, t)$  equal to zero on the seabed,

51 i.e.,  $\Psi(x, y, -h, t) = 0$ . In the IGN theory, we assume that  $\Psi$  is given by

$$\Psi(x, y, z, t) = \sum_{m=1}^K \Psi_m(x, y, t) f_m(\gamma), \quad (2)$$

52 where  $f_m(\gamma) = \gamma^{2m-1}$ ,  $\gamma = (z + h)/(\eta + h)$  and  $\Psi_m$  are the unknown stream function  
53 coefficients which are calculated as part of the solution.

The IGN equations are given by two canonical equations for the free-surface elevation  $\eta(x, y, t)$  and the surface velocity potential  $\hat{\phi}(x, y, t)$ :

$$\eta_{,t} + \sum_{m=1}^K f_m(1) \nabla \cdot \Psi_m = 0, \quad (3a)$$

$$\hat{\phi}_{,t} = -\nabla \cdot \frac{\partial T}{\partial(\nabla\eta)} + \frac{\partial T}{\partial\eta} - g\eta, \quad (3b)$$

54 where  $T$  is the kinetic energy given by

$$\begin{aligned} T = \frac{1}{2} \sum_{m=1}^K \sum_{n=1}^K \{ & \theta A_{mn} (\nabla \cdot \Psi_m) (\nabla \cdot \Psi_n) \\ & + 2B_{mn} (\nabla \cdot \Psi_m) (\Psi_n \cdot \nabla h) - 2B_{mn}^1 (\nabla \cdot \Psi_m) (\Psi_n \cdot \nabla \theta) \\ & + \frac{1}{\theta} C_{mn} [\Psi_m \cdot \Psi_n + (\nabla h \cdot \Psi_m) (\nabla h \cdot \Psi_n)] - \frac{2}{\theta} C_{mn}^1 (\nabla h \cdot \Psi_m) (\nabla \theta \cdot \Psi_n) \\ & + \frac{1}{\theta} C_{mn}^2 (\nabla \theta \cdot \Psi_m) (\nabla \theta \cdot \Psi_n) \}, \end{aligned} \quad (4)$$

where  $\theta = \eta + h$  and

$$A_{mn} = \int_0^1 f_m(\gamma) f_n(\gamma) d\gamma, \quad (5a)$$

$$B_{mn} = \int_0^1 f_m(\gamma) f'_n(\gamma) d\gamma, \quad B_{mn}^1 = \int_0^1 \gamma f_m(\gamma) f'_n(\gamma) d\gamma, \quad (5b)$$

$$C_{mn} = \int_0^1 f'_m(\gamma) f'_n(\gamma) d\gamma, \quad C_{mn}^1 = \int_0^1 \gamma f'_m(\gamma) f'_n(\gamma) d\gamma, \quad (5c)$$

$$C_{mn}^2 = \int_0^1 \gamma^2 f'_m(\gamma) f'_n(\gamma) d\gamma. \quad (5d)$$

55 Details of the derivation of the IGN equations can be found in Kim et al. (2001, 2003).

56 The IGN equations are completed by stating the relation between the surface velocity  
57 potential  $\hat{\phi}(x, y, t)$  and the stream function coefficients  $\Psi_m$  ( $m = 1, 2, \dots, K$ ):

$$f_m(1) \nabla \hat{\phi} = -\nabla \frac{\partial T}{\partial(\nabla \cdot \Psi_m)} + \frac{\partial T}{\partial \Psi_m} \quad (m = 1, 2, \dots, K). \quad (6)$$

Equations (3) and (6) constitute the three-dimensional IGN equations, and they are used to solve for  $\eta$ ,  $\hat{\phi}$  and  $\Psi_m$  ( $m = 1, 2, \dots, K$ ). In addition,  $K$  stands for the level of IGN equations. For example,  $K = 1, K = 2, K = 3$  represent IGN-1 equations, IGN-2 equations, IGN-3 equations, respectively. Here, we focus on the IGN-2 equations.

### 3. Solution Algorithm

For the IGN-2 equations, Eq. (6) in the  $x$  and  $y$  directions can be expressed by

$$\tilde{\mathbf{A}}^u \xi^u_{,xx} + \tilde{\mathbf{B}}^u \xi^u_{,x} + \tilde{\mathbf{C}}^u \xi^u = \tilde{\mathbf{f}}^u, \quad (7a)$$

$$\tilde{\mathbf{A}}^v \xi^v_{,yy} + \tilde{\mathbf{B}}^v \xi^v_{,y} + \tilde{\mathbf{C}}^v \xi^v = \tilde{\mathbf{f}}^v, \quad (7b)$$

where the superscript  $u$  and  $v$  are used to differentiate the  $x$  and  $y$  directions in Eq. (6),  $\xi^u = [\psi_1^u, \psi_2^u]^T$  and  $\xi^v = [\psi_1^v, \psi_2^v]^T$ . The subscript after comma stands for differentiation with respect to the indicated variable.  $\xi^u_{,x}$  and  $\xi^u_{,xx}$ , for example, indicate the first and second derivatives of  $\xi^u$ , respectively.

In Eq. (7),  $\tilde{\mathbf{A}}^u, \tilde{\mathbf{B}}^u, \tilde{\mathbf{C}}^u, \tilde{\mathbf{A}}^v, \tilde{\mathbf{B}}^v$  and  $\tilde{\mathbf{C}}^v$  are  $2 \times 2$  matrices. They are functions of  $h, \eta$  and their spatial derivatives.  $\tilde{\mathbf{f}}^u$  and  $\tilde{\mathbf{f}}^v$  are 2-dimensional vectors.  $\tilde{\mathbf{f}}^u$  are functions of  $h, \eta, \xi^v$  and their spatial derivatives.  $\tilde{\mathbf{f}}^v$  are functions of  $h, \eta, \xi^u$  and their spatial derivatives.

The finite central-difference method is used here for spatial derivatives. The  $(x, y)$  domain is uniformly discretized in the calculations by  $(\Delta x, \Delta y)$  intervals. The discretized point on the grid is denoted by  $x_i = i\Delta x$  for  $i = 1, 2, \dots, n_x$  and  $y_j = j\Delta y$  for  $j = 1, 2, \dots, n_y$ . Time is discretized with intervals of  $\Delta t$  such that  $t_k = k\Delta t$  for  $k = 1, 2, \dots$ .

For a given  $j$ ,  $\xi^u(i, j)$  ( $i = 1, 2, \dots, n_x$ ) can be obtained by solving Eq. (7a). Similarly, for a given  $i$ , we can obtain  $\xi^v(i, j)$  ( $j = 1, 2, \dots, n_y$ ) from Eq. (7b). Further details of the numerical solution of Eq. (7a) can be found in Zhao et al. (2014).

We use the fourth-order Adams predictor-corrector scheme to march in time. They are

$$\eta^k = \eta^{k-1} + (55\eta_t^{k-1} - 59\eta_t^{k-2} + 37\eta_t^{k-3} - 9\eta_t^{k-4})\Delta t/24, \quad (8a)$$

$$\eta^k = \eta^{k-1} + (9\eta_t^k + 19\eta_t^{k-1} - 5\eta_t^{k-2} + \eta_t^{k-3})\Delta t/24, \quad (8b)$$

77 where  $k$  indicates the time step in  $t_k = k\Delta t$  for  $k = 1, 2, \dots$ . Similarly,  $\hat{\phi}$  can also be predicted  
 78 and corrected.

79 The wave maker is based on the solution of the linearised IGN-2 equations and this will  
 80 be discussed in the next Section. For the cases studied here, two wave-absorbing regions  
 81 are used: one near the wave-maker to prevent the reflected waves from interfering with the  
 82 wave-maker, and the other one to absorb waves at the opposite end of the domain, see Zhao  
 83 et al. (2014, 2015a) for more details.

#### 84 4. Solution of the linearised IGN-2 equations

85 To obtain the solution of the linearised IGN-2 equations, we use the one-dimensional  
 86 (horizontal component) IGN equations and set the water depth to a constant  $h(x) = d$ .  
 87 First, we linearize Eq. (3b) to obtain

$$\hat{\phi}_{,t} = -g\eta(x, t). \quad (9)$$

88 We assume that the change of the wave surface elevation can be described by a cosine  
 89 function:

$$\eta = A\cos(k(x - ct)), \quad (10)$$

90 where  $k$  is the wave number and  $c$  the wave speed. Then, from Eq. (9)

$$\hat{\phi} = \frac{Ag}{ck}\sin(k(x - ct)). \quad (11)$$

We can also obtain the linearized form of Eq. (6). They are given as

$$-\hat{\phi}_{,x}(x, t) + \frac{\psi_1(x, t)}{d} + \frac{\psi_2(x, t)}{d} - \frac{1}{3}d\psi_1^{(2,0)}(x, t) - \frac{1}{5}d\psi_2^{(2,0)}(x, t) = 0, \quad (12a)$$

$$-\hat{\phi}_{,x}(x, t) + \frac{\psi_1(x, t)}{d} + \frac{9\psi_2(x, t)}{5d} - \frac{1}{5}d\psi_1^{(2,0)}(x, t) - \frac{1}{7}d\psi_2^{(2,0)}(x, t) = 0. \quad (12b)$$

We assume that the coefficient  $\psi_1$  and  $\psi_2$  change as

$$\psi_1 = Q_1\cos(k(x - ct)), \quad (13a)$$

$$\psi_2 = Q_2\cos(k(x - ct)). \quad (13b)$$



Substituting Eqs. (13) and (11) into Eq. (12) gives

$$-\frac{Ag}{c} + \frac{Q_1}{d} + \frac{1}{3}dk^2Q_1 + \frac{Q_2}{d} + \frac{1}{5}dk^2Q_2 = 0, \quad (14a)$$

$$-\frac{Ag}{c} + \frac{Q_1}{d} + \frac{1}{5}dk^2Q_1 + \frac{9Q_2}{5d} + \frac{1}{7}dk^2Q_2 = 0. \quad (14b)$$

Equations (14) can be written as

$$Q_1 = -\frac{15Adg(-14 + d^2k^2)}{2c(105 + 45d^2k^2 + d^4k^4)}, \quad (15a)$$

$$Q_2 = \frac{35Ad^3gk^2}{2c(105 + 45d^2k^2 + d^4k^4)}. \quad (15b)$$

91 On the other hand, Eq. (3a) can be written as

$$\eta^{(0,1)}(x, t) + \psi_1^{(1,0)}(x, t) + \psi_2^{(1,0)}(x, t) = 0. \quad (16)$$

92 Substituting Eqs. (15) and (13) into Eq. (16) gives

$$c^2 = \frac{5(21dg + 2d^3gk^2)}{105 + 45d^2k^2 + d^4k^4}. \quad (17)$$

93 The nondimensional form of  $c^2$  is

$$\bar{c}^2 = \frac{5(21 + 2\bar{k}^2)}{105 + 45\bar{k}^2 + \bar{k}^4}, \quad (18)$$

94 where the constant water depth  $d$  and gravitational acceleration  $g$  are used to obtain the  
95 nondimensional Eq. (18).

96 The Airy wave theory (or linear water wave theory) gives the linear dispersion relation  
97 (see for example Wiegel (1964))

$$\bar{c}_{Airy}^2 = \tanh(\bar{k})/\bar{k}. \quad (19)$$

98 In Fig. 1, it is shown that the relation between  $c/c_{Airy}$  and  $kh$  is predicted by the linearised  
99 IGN-2 equations. We observe that the IGN-2 equations give errors of less than 2% in the  
100 phase velocity from shallow-water depths up to  $kd = 4.87$ . We also note that the IGN-2  
101 equations have no restriction on the wave amplitude. They can be used to simulate waves  
102 up to the breaking point.

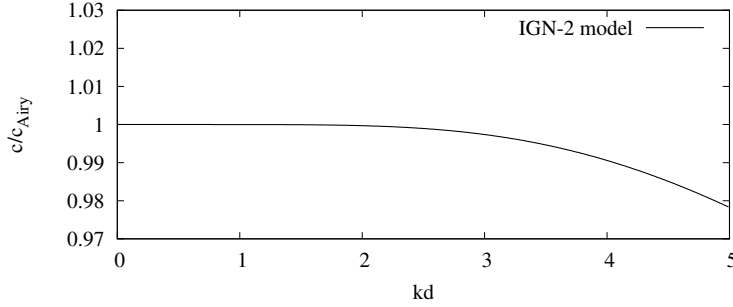


Figure 1: Linear dispersion relation of the IGN-2 model.

## 103 5. Test cases

104 In this section, we will present results of the IGN-2 equations in three dimensions for three  
 105 different cases. The results are compared with some existing laboratory experiments, and  
 106 with the available theoretical and numerical solutions of the problems.

### 107 5.1. Wave evolution in a closed basin

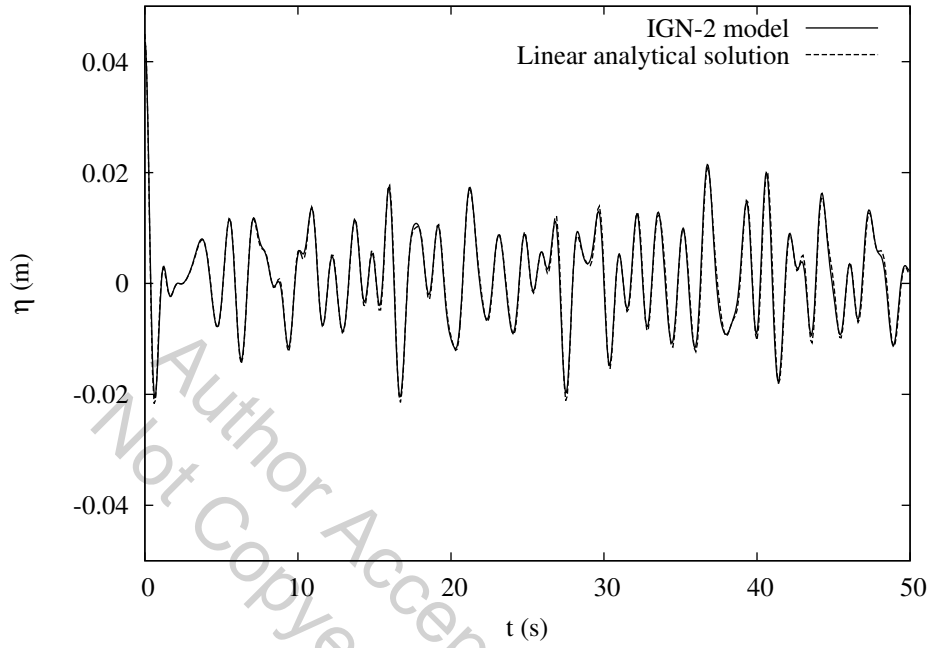
108 To study the accuracy of the three-dimensional IGN-2 equations and the numerical model  
 109 used here, we first consider the problem of wave evolution in a closed basin with  $L_x = L_y =$   
 110  $7.5m$ , where  $L_x$  and  $L_y$  are the length and width of the basin, respectively.

111 The domain is extended between  $-L_x/2 \leq x \leq L_x/2$  and  $-L_y/2 \leq y \leq L_y/2$  with  
 112 reflective vertical walls. The initial condition is a surface elevation of Gaussian shape  $\eta_0(x, y)$   
 113 above an otherwise constant water depth  $h_0 = 0.45m$ .  $\eta_0(x, y)$  is defined by

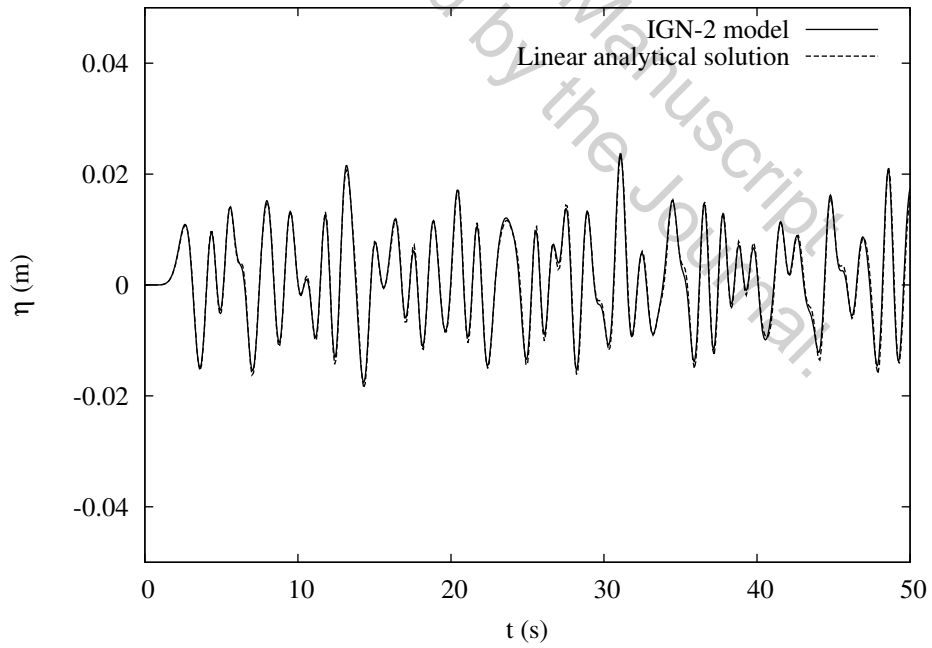
$$\eta_0(x, y) = H_0 \exp[-2(x^2 + y^2)], \quad (20)$$

114 where  $H_0 = 0.1h_0 = 0.045m$  in this case. Grid size of  $\Delta x = \Delta y = 0.15m$  and time step size  
 115 of  $\Delta t = 0.05s$  are used. The IGN-2 results are compared with the linear analytical solution  
 116 of this problem (Wei and Kirby, 1995). The comparison on wave elevation at two points is  
 117 shown in Fig. 2. These two points are: point (a) at  $x = 0m$  and  $y = 0m$ , i.e., the center of  
 118 the computational domain, and point (b) at  $x = -L_x/2$  and  $y = -L_y/2$ , i.e., the corner.

119 Due to the small initial wave amplitude,  $H_0 = 0.1h_0$ , the agreement between IGN-2 results  
 120 and the linear solution of the problem is very good. The initial elevation is symmetric about



(a)  $x = 0\text{m}$  and  $y = 0\text{m}$



(b)  $x = -L_x/2$  and  $y = -L_y/2$

Figure 2: Time histories of wave elevation at two points ((a) center and (b) corner of the basin).

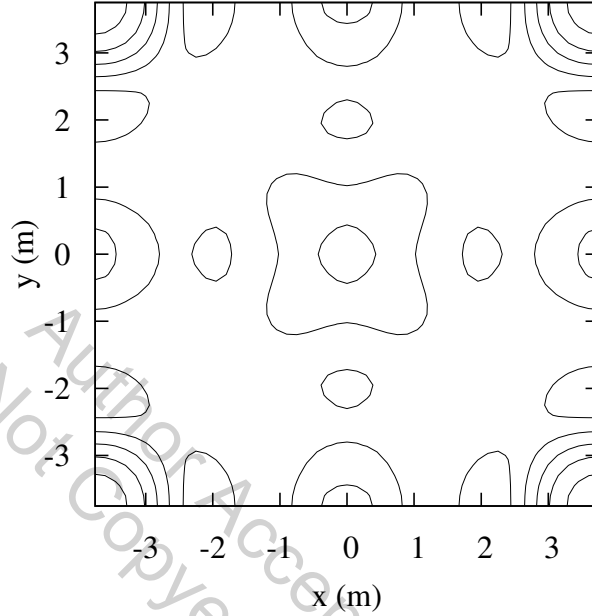


Figure 3: Surface contour of the IGN-2 model, illustrating rotational symmetry of evolving waves.

121 the center of the basin ( $x = 0m$ ,  $y = 0m$ .) As a result, the surface elevation at anytime should  
 122 be symmetric about the center. The contours of the free surface at  $t = 50s$  are calculated  
 123 by the IGN-2 equations; they are shown in Fig. 3. We observe that the contours of wave  
 124 evolution is symmetric about the center of the basin.

125 We also checked the mass conservation. Since no water can escape the numerical basin,  
 126 the water volume should remain constant in our calculations, and it is indeed determined to  
 127 be constant. In addition, the computational time of this case is within 1 minutes on Inter(R)  
 128 Core(TM) i7-7700 CPU @ 3.60GHz processor.

### 129 5.2. Wave transformation over a circular shoal (Chawla and Kirby, 1996)

130 Chawla and Kirby (1996) conducted a series of physical experiments for wave transfor-  
 131 mation over a circular shoal. Their experiments consist of test cases of regular waves and  
 132 directional random waves, including breaking and nonbreaking waves. To study the com-

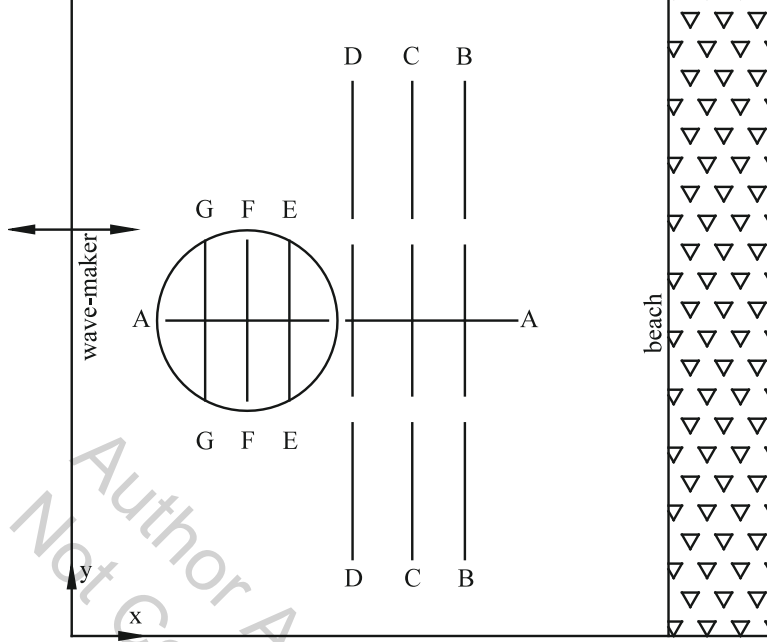


Figure 4: Experimental setup of wave transformation over a circular shoal of Chawla and Kirby (1996).

133 bined wave refraction/diffraction in two horizontal dimensions, we present comparisons with  
 134 the nonbreaking monochromatic wave cases.

135 The dimensions of the physical wave tank used by Chawla and Kirby (1996) is  $0 \leq x \leq$   
 136  $20m$  and  $0 \leq y \leq 18.2m$ ; a circular shoal is placed on an otherwise flat bottom in the basin,  
 137 as shown in Fig. 4. The center of the shoal is located at  $x = 5m$  and  $y = 8.98m$ . The  
 138 perimeter of the shoal is defined by

$$(x - 5)^2 + (y - 8.98)^2 = (2.57)^2. \quad (21)$$

139 The water depth on the submerged shoal is given by

$$h = h_0 + 8.73 - \sqrt{82.81 - (x - 5)^2 - (y - 8.98)^2}, \quad (22)$$

140 where  $h_0 = 0.45m$  is the constant water depth of the basin.

141 In our numerical calculations, we extend the domain to  $-2 \leq x \leq 33m$  to avoid reflections  
 142 contaminate the interior results. We confine our attention to waves in the range of  $0 \leq x \leq$   
 143  $20m$ . Whereas  $-2 \leq x \leq 2m$  region is used to absorb the reflected waves by the shoal back  
 144 to the wave-maker, and  $29 \leq x \leq 33m$  region is used to absorb the waves on the right end

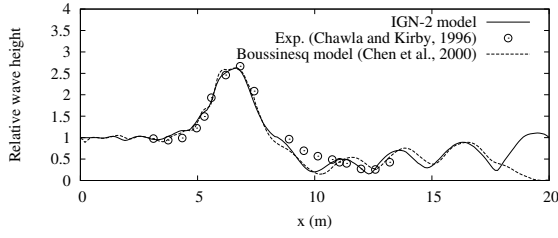
145 of the domain. At  $x = -2m$ , monochromatic waves are generated, and they propagate in  
146 the positive  $x$  direction over the circular shoal. The wave height of the incoming waves is  
147  $H_0 = 1.18cm$ , and the wave period is  $T = 1.0s$ . At the wave maker,  $kh = 1.89$ , which is  
148 within the limits of the IGN-2 equations.

149 On the top of the circular shoal, the water depth is  $h = 8cm$ . We choose a uniform  
150 grid spacing of  $\Delta x = \Delta y = 0.1m$  in both the  $x$  and  $y$  directions. A time step of  $\Delta t =$   
151  $0.0333s$  is used. The comparison of the relative wave height ( $H/H_0$ ) between the IGN-  
152 2 equations and the fully nonlinear Boussinesq equations of Chen et al. (2000), and the  
153 laboratory measurements of Chawla and Kirby (1996) at different locations in the tank is  
154 shown in Fig. 5.

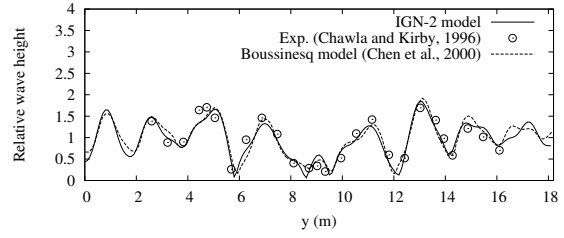
155 From Fig. 5, a close agreement between the IGN-2 results and the experimental data  
156 of Chawla and Kirby (1996) is observed. In this case, the  $H/H_0$  ratio reaches the value of  
157  $H/H_0 = 2.7$ , as seen in Fig. 5(a). The results for  $H/H_0$  from the Boussinesq equations  
158 (Chen et al., 2000) go to zero at the end of tank, while IGN-2 results do not approach  
159 zero. Note that the numerical wave tank in Chen et al. (2000) is  $20m$  long and waves are  
160 absorbed before  $x = 20m$ . In our calculations, however, the numerical tank is much longer  
161 and the waves are not absorbed at  $x = 20m$ . The close agreement between the IGN-2 and  
162 the Boussinesq equations (Chen et al., 2000) observed along the transects at  $x = 3.8m$ ,  
163  $x = 5.0m$ ,  $x = 6.2m$ ,  $x = 8.0m$ ,  $x = 9.7m$  and  $x = 11.2m$  (see Figs. 5(b)-5(g)) implies  
164 that the combined refraction/diffraction effects are captured successfully by these equations.  
165 The shoal center is located at the  $y = 8.98m$  (the width of the tank is  $18.2m$ ), which is  
166 slightly closer to one of the side walls ( $y = 0m$ ). Therefore, the distribution of wave height  
167 in the  $y$  direction is not symmetric; this can be observed in Figs. 5(b)-5(g). In addition, the  
168 computational time is less than 10 minutes.

### 169 5.3. Wave transformation over a semi-circular shoal (Whalin, 1971)

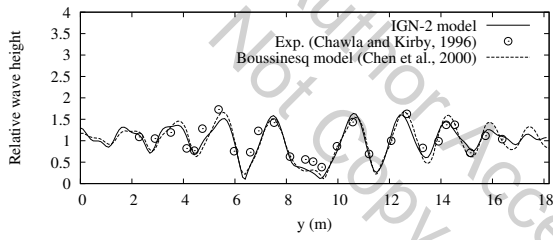
Whalin (1971) conducted a series of laboratory experiments on wave convergence over a  
bottom topography. The size of the tank is  $0m \leq x \leq 25.603m$  and  $0m \leq y \leq 6.096m$ . The



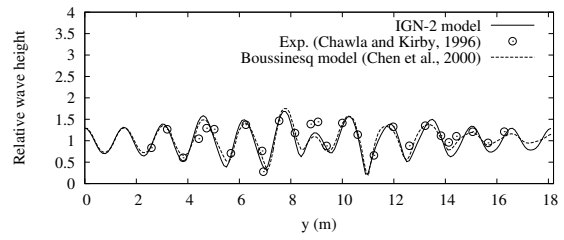
(a) Transect A-A ( $y = 8.98\text{m}$ )



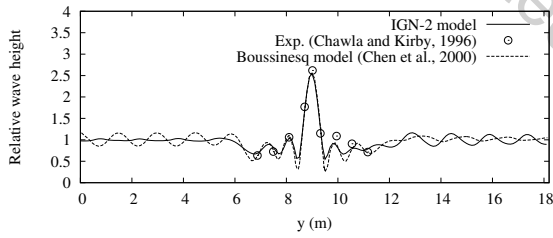
(b) Transect B-B ( $x = 11.2\text{m}$ )



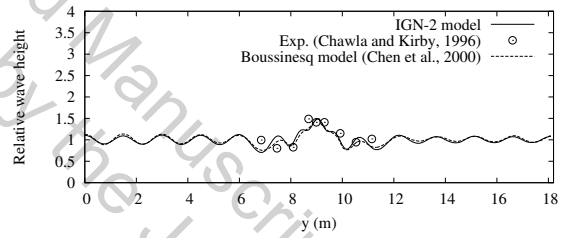
(c) Transect C-C ( $x = 9.7\text{m}$ )



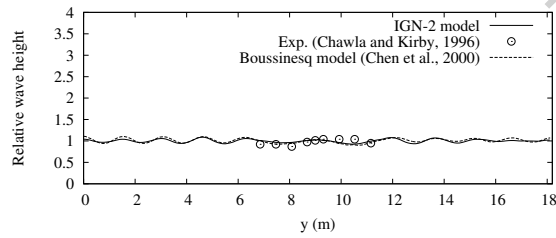
(d) Transect D-D ( $x = 8.0\text{m}$ )



(e) Transect E-E ( $x = 6.2\text{m}$ )



(f) Transect F-F ( $x = 5.0\text{m}$ )



(g) Transect G-G ( $x = 3.8\text{m}$ )

Figure 5: Comparison of relative wave height calculated by the IG-N-2 model with laboratory measurements of Chawla and Kirby (1996) and numerical results of Chen et al. (2000).

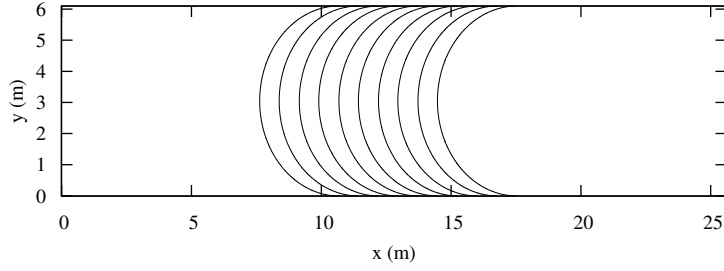


Figure 6: Setup of the wave tank of Whalin (1971).

bathymetry is shown in Fig. 6. The equations approximating the bathymetry are given as follows (Whalin, 1971):

$$h(x, y) = \begin{cases} 0.4572 & (x \leq 10.67 - G) \\ 0.4572 + \frac{1}{25}(10.67 - G - x) & (10.67 - G \leq x \leq 18.28 - G) \\ 0.1524 & (x \geq 18.28 - G) \end{cases} \quad (23a)$$

$$G(y) = \sqrt{y(6.096 - y)} \quad (0 \leq y \leq 6.096), \quad (23b)$$

170 where  $x$  and  $y$  are measured in meter. A semi-circular shoal is used to connect the deep part  
171 of the basin with the shallow part.

172 Whalin (1971) conducted three sets of experiments by generating waves in the deeper part  
173 of the model with periods of 1s, 2s and 3s. This case is considered by many as a benchmark  
174 experiment for their numerical models. For example, Rygg (1988), Kennedy and Fenton  
175 (1996), Li and Fleming (1997), Eskilsson and Sherwin (2006), Engsig-Karup et al. (2008),  
176 Bingham et al. (2009), Young et al. (2009), and others, compared their numerical results  
177 with these experimental data.

178 Here, we use the results of Rygg (1988), Li and Fleming (1997) and Bingham et al.  
179 (2009) to perform a comparative study. Rygg (1988) tested the classical Boussinesq equa-  
180 tions against the experimental data for nonlinear waves of periods 2s and 3s. Li and Fleming  
181 (1997) developed a three-dimensional multigrid model for fully nonlinear water waves. Bing-  
182 ham et al. (2009) tested the highly accurate Boussinesq-type model against some of the  
183 experimental data. The incoming wave parameters studied here are shown in Table 1.



Case	T(s)	A(cm)	Boussinesq model (Rygg, 1988)	Fully nonlinear multigrid model (Li and Fleming, 1997)	Highly accurate Boussinesq models (Bingham et al., 2009)
1	1	0.97	—	Fig. 10	—
2	1	1.95	—	Fig. 11	Fig. 6
3	2	0.75	Fig. 5	Fig. 12	Fig. 7
4	2	1.06	Fig. 6	Fig. 13	—
5	2	1.49	Fig. 7	Fig. 14	—
6	3	0.68	Fig. 8	Fig. 15	Fig. 8
7	3	0.98	Fig. 9	Fig. 16	—
8	3	1.46	Fig. 10	Fig. 17	—

Table 1: Wave conditions of Whalin (1971) and numerical models of others

184 Due to the symmetry along  $y = 3.048m$ , only half of the  $y$  region is considered in our  
185 calculations. In all the numerical calculations, the spatial step is  $\Delta x = \Delta y = 0.1016m$  and  
186 the time step is  $\Delta t = 0.025s$ . An FFT analysis of the time series was made for each grid at  
187 the central line of the wave tank ( $y = 3.048m$ ). The numerical results are compared with the  
188 experimental data and presented in Figs. 7-14.

189 In Case 1 ( $T = 1.0s$  and  $a = 0.0097m$ ), shown in Table 1, the IGN-2 results are close to  
190 the experimental data, see Fig. 7. As waves refract over the topography and focus along the  
191 centerline of the tank, a significant amount of energy is transferred into the higher-harmonic  
192 components. We also observe that the agreement of the IGN-2 results with the experimental  
193 data is better than the results of Li and Fleming (1997).

194 For Case 2 ( $T = 1.0s$  and  $a = 0.0195m$ ), the IGN-2 results are also in good agreement  
195 with the experimental data, see Fig. 8. The highly accurate Boussinesq results (Bingham  
196 et al., 2009) agree very well with the IGN-2 results. The small differences between the IGN-2  
197 results and the highly accurate Boussinesq results are mainly caused by the reflections from

198 the right side of the Boussinesq calculations. In the IGN-2 calculations, the length of the tank  
199 is set long enough to avoid reflections. We also observe that both the IGN-2 results and the  
200 highly accurate Boussinesq results are in better agreement with the laboratory measurements  
201 than the fully nonlinear multigrid model results of Li and Fleming (1997).

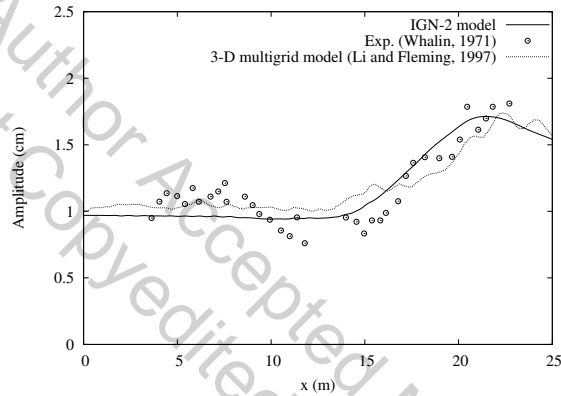
202 For the case of  $T = 2s$ , the IGN-2 results are shown in Figs. 9-11. We observe that  
203 the IGN-2 results agree well with the experimental data. The solutions of the Boussinesq  
204 equations (Rygg, 1988) and the fully nonlinear multigrid model (Li and Fleming, 1997) are  
205 used for comparisons. For Cases 3-5, the fully nonlinear multigrid results (Li and Fleming,  
206 1997) do not agree well with the experimental data. The results from Boussinesq equations  
207 (Rygg, 1988) are better than the fully nonlinear multigrid model results (Li and Fleming,  
208 1997). The results of the higher-harmonic amplitudes predicted by the Boussinesq equations  
209 (Rygg, 1988) are lower than those of the IGN-2.

210 For Case 3, we compare the IGN-2 results with the highly accurate Boussinesq results  
211 (Bingham et al., 2009). Very good agreement is observed, and this indicates that the IGN-2  
212 results here are more accurate than the Boussinesq equations of Rygg (1988) in this case.  
213 We also observe that when the wave amplitude increases, the second harmonic amplitudes  
214 increase significantly, see Figs. 9(b), 10(b), 11(b). Similarly, the third harmonic amplitudes  
215 increase. Keeping more harmonic components in the analysis seems to be more reasonable,  
216 and in our calculations we considered up to the fifth harmonics.

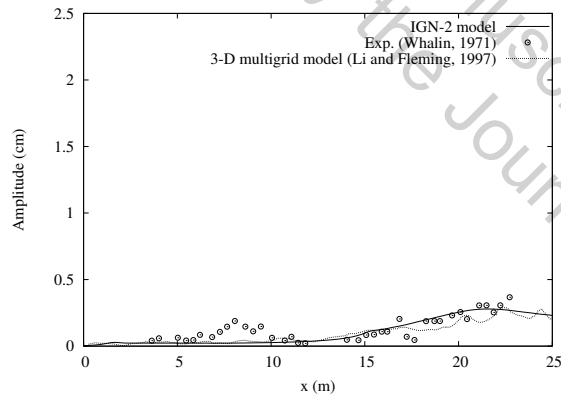
217 For the case of  $T = 3s$ , the IGN-2 results are shown in Figs. 12-14, and they agree  
218 well with the experimental data. It is also observed that there are some differences between  
219 the numerical results of all models and the experimental data. In the paper by Bingham  
220 et al. (2009), they reproduced Case 6 and they also observed that there are some differences  
221 between their highly accurate Boussinesq results and the experimental data. For the cases of  
222  $T = 3s$ , there is significant reflection from the right side during the experiments. The reflected  
223 energy propagates back to the wave maker and possibly interfere with the wave generation in  
224 the physical experiments. In our numerical calculation, we use two wave-absorbing regions  
225 as mentioned at the end of Section 3. This may explain the larger differences seen for this

226 case.

227 For Case 6, the results of highly accurate Boussinesq (Bingham et al., 2009) and the present  
228 IGN-2 results are in good agreement. For Cases 6-8, the results from Boussinesq equations  
229 of Rygg (1988) and the present IGN-2 results are in good agreement. The fully nonlinear  
230 multigrid model results of Li and Fleming (1997) do not show good accuracy compared with  
231 the other numerical results. In addition, the computational time of each case is less than 6  
minutes.



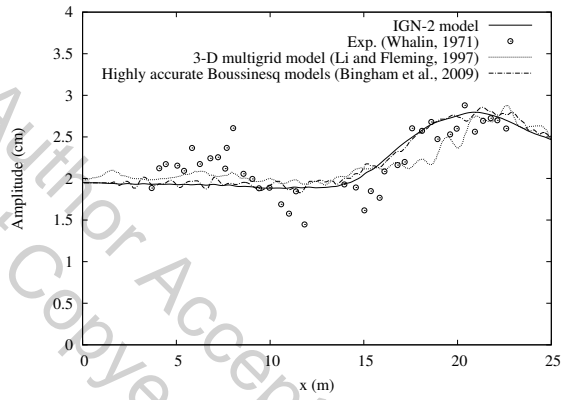
(a) 1st harmonic



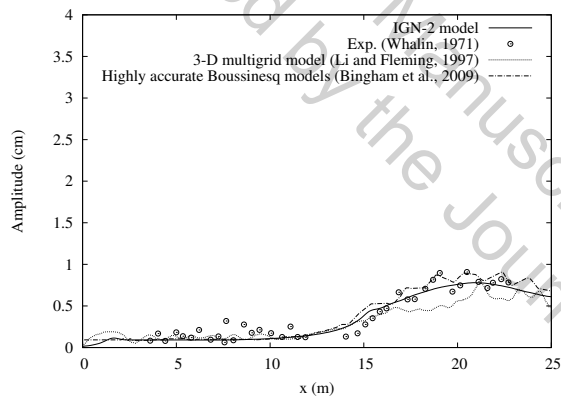
(b) 2nd harmonic

Figure 7: Wave amplitudes along the centerline of the wave tank for Case 1.

232

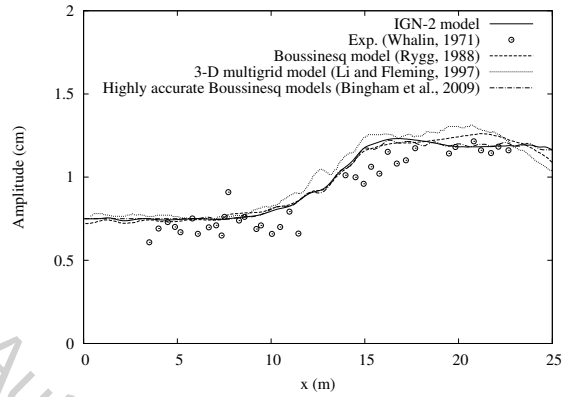


(a) 1st harmonic

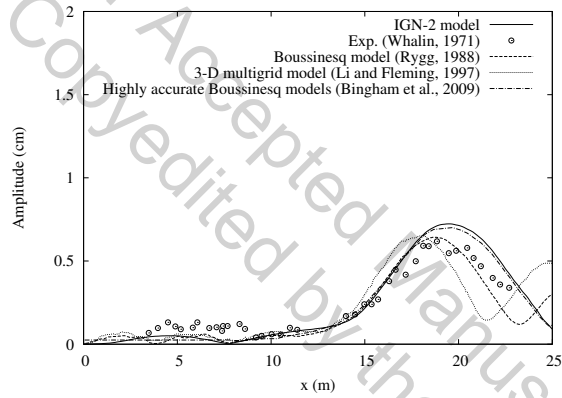


(b) 2nd harmonic

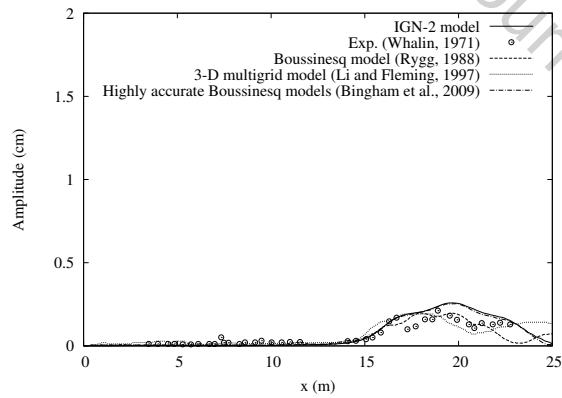
Figure 8: Wave amplitudes along the centerline of the wave tank for Case 2.



(a) 1st harmonic

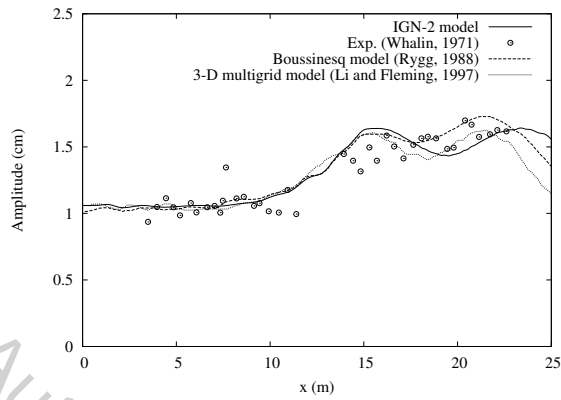


(b) 2nd harmonic

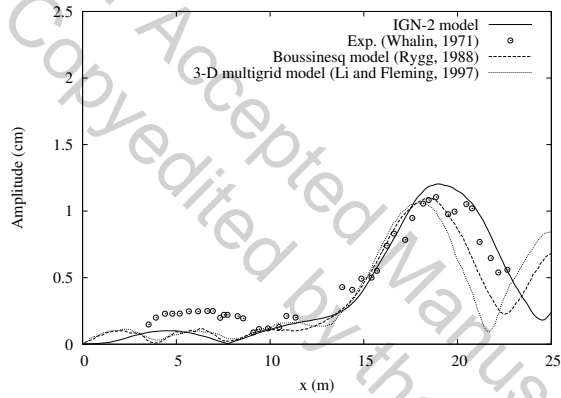


(c) 3rd harmonic

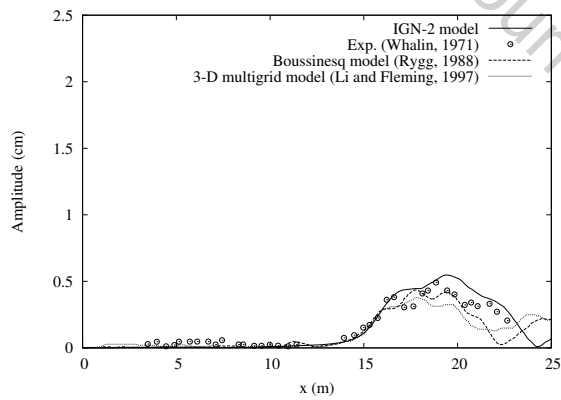
Figure 9: Wave amplitudes along the centerline of the wave tank for Case 3.



(a) 1st harmonic

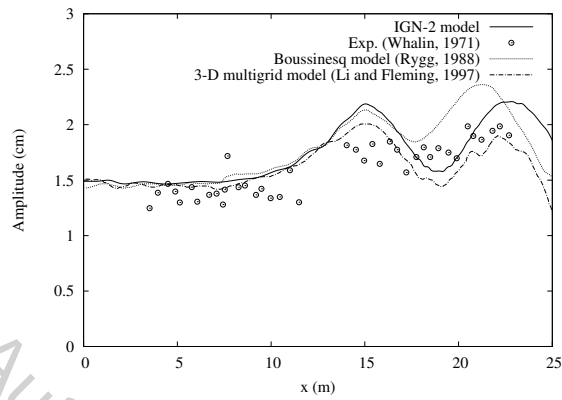


(b) 2nd harmonic

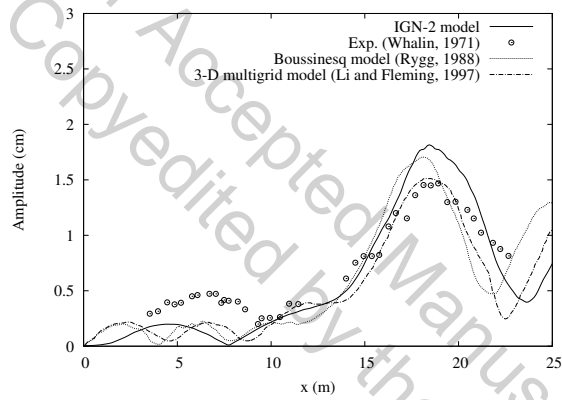


(c) 3rd harmonic

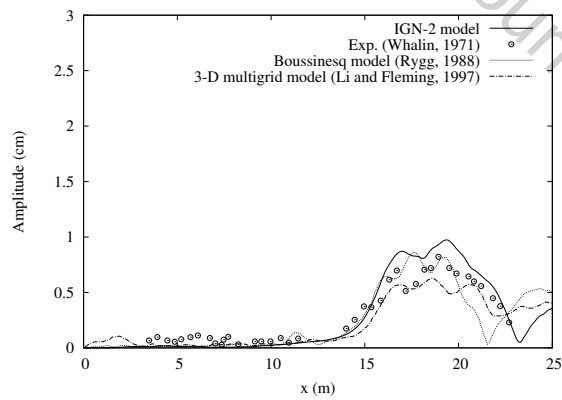
Figure 10: Wave amplitudes along the centerline of the wave tank for Case 4.



(a) 1st harmonic

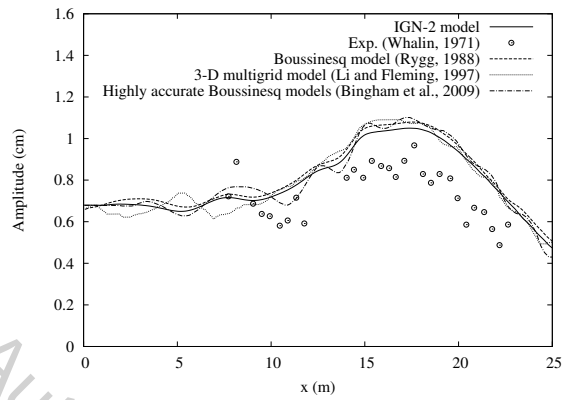


(b) 2nd harmonic

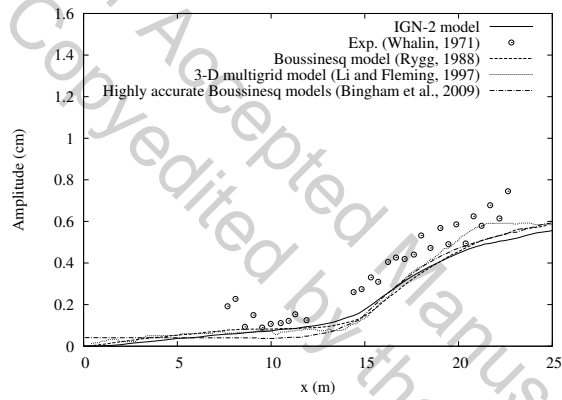


(c) 3rd harmonic

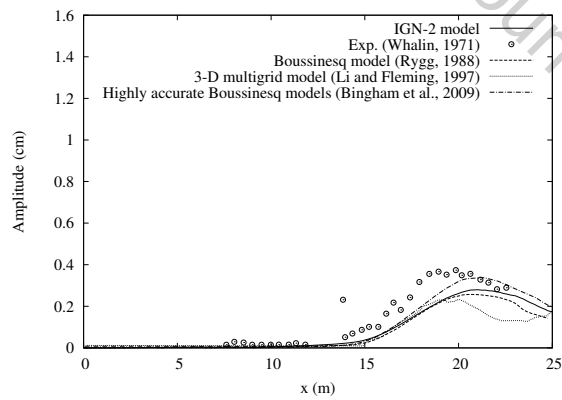
Figure 11: Wave amplitudes along the centerline of the wave tank for Case 5.



(a) 1st harmonic



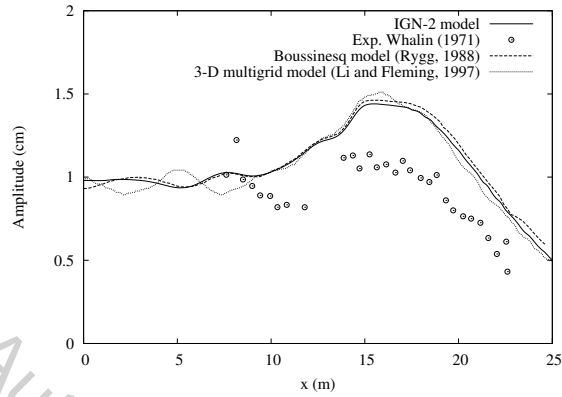
(b) 2nd harmonic



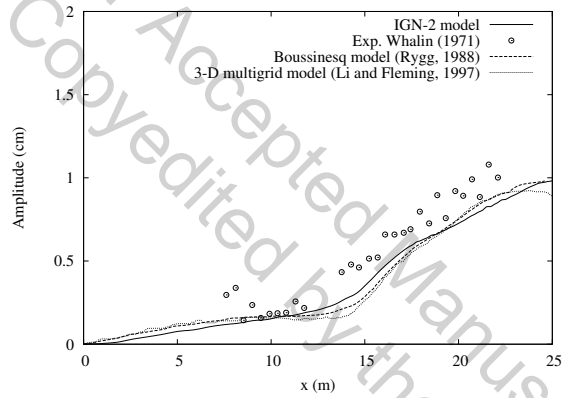
(c) 3rd harmonic

Figure 12: Wave amplitudes along the centerline of the wave tank for Case 6.

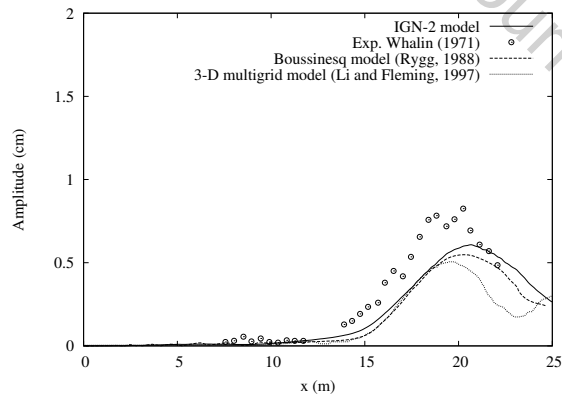




(a) 1st harmonic

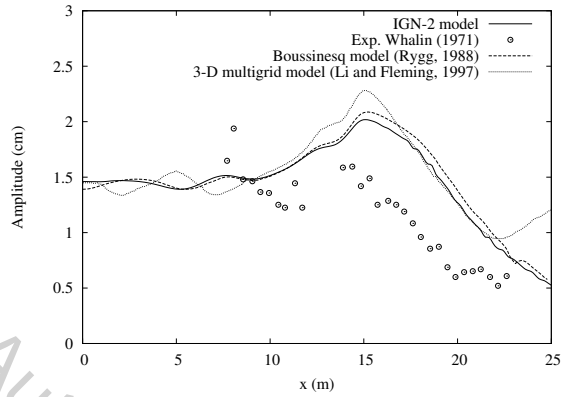


(b) 2nd harmonic

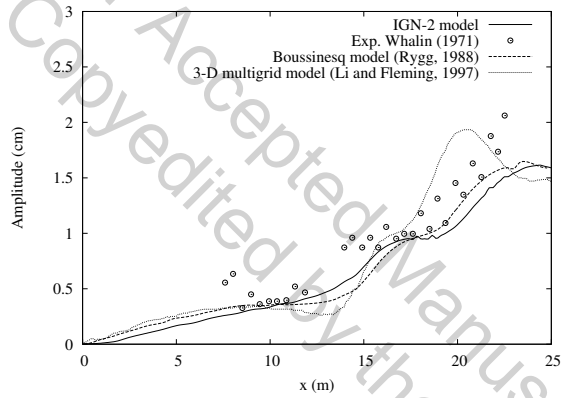


(c) 3rd harmonic

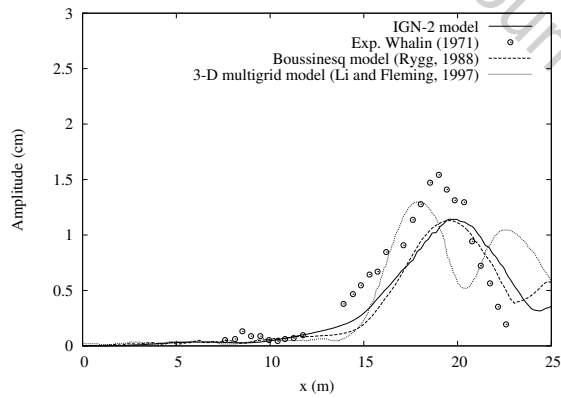
Figure 13: Wave amplitudes along the centerline of the wave tank for Case 7.



(a) 1st harmonic



(b) 2nd harmonic



(c) 3rd harmonic

Figure 14: Wave amplitudes along the centerline of the wave tank for Case 8.

## 233 6. Conclusions

234 A numerical model to solve the three-dimensional IGN-2 equations are introduced and  
235 applied to some wave diffraction and refraction problems. The solution of the IGN-2 equations  
236 are also provided. Here, we present three test cases to study the accuracy of the IGN-2  
237 equations. The first case is on wave evolution in a closed basin. The IGN-2 results show  
238 good agreement with the linear analytical solution for small wave heights. In the second  
239 test case, we numerically recreated the experiments of Chawla and Kirby (1996) on wave  
240 diffraction due to a three-dimensional circular shoal. A close agreement between the IGN-  
241 2 equations, the laboratory data (Chawla and Kirby, 1996) and the Boussinesq equations  
242 (Chen et al., 2000) is observed.

243 In the last test case, we reproduce the experiments of Whalin (1971) numerically. Whalin  
244 (1971) conducted three sets of experiments by generating waves with periods of  $1s$ ,  $2s$  and  
245  $3s$ , and also with different amplitudes, see Table 1. In all these cases, the fully nonlinear  
246 multigrid model (Li and Fleming, 1997) does not produce accurate results but the IGN-2  
247 results agree well with the highly accurate Boussinesq results (Bingham et al., 2009) and the  
248 experimental data. It is shown that the IGN-2 results are very accurate for different wave  
249 lengths and wave amplitudes. For cases when  $T = 2s$ , the Boussinesq equations (Rygg, 1988)  
250 underpredict the results compared with the IGN-2 results and the highly accurate Boussinesq  
251 results (Bingham et al., 2009). Only for cases with  $T = 3s$ , the Boussinesq equations (Rygg,  
252 1988) provide close results with the IGN-2. This is not surprising because the Boussinesq  
253 equations of Rygg (1988) assume weak dispersion. The strongly nonlinear IGN-2 equations  
254 give errors of less than 2% in phase velocity from shallow-water depths up to  $kd = 4.87$ . The  
255 IGN-2 equations do not have a restriction on the wave amplitude; they can simulate waves  
256 up to breaking.

257 It is concluded that for many coastal engineering problems, the IGN-2 equations are more  
258 suitable than a number of other perturbation-based methods because of the higher accuracy  
259 and simplicity of the theory.

260 **Acknowledgement**

261 The work is supported by the National Natural Science Foundation of China (Nos. 11572093,  
262 11772099, 51490671), International Science and Technology Cooperation Project sponsored  
263 by National Ministry of Science and Technology of China (No. 2012DFA70420), the Special  
264 Fund for Basic Scientific Research of Central Colleges (Harbin Engineering University), the  
265 Heilongjiang Touyan Innovation team Program.

266 **References**

267 **References**

- 268 Bingham, H.B., Madsen, P.A., Fuhrman, D.R., 2009. Velocity potential formulations of  
269 highly accurate Boussinesq-type models. *Coastal Engineering* 56, 467–478.
- 270 Chawla, A., Kirby, J.T., 1996. Wave transformation over a submerged shoal. Technical  
271 Report. CACR Rep. No. 96-03, Dept. of Civ. Engrg., University of Delaware, Newark, Del.
- 272 Chen, Q., Kirby, J.T., Dalrymple, R.A., Kennedy, A.B., Chawla, A., 2000. Boussinesq  
273 modeling of wave transformation, breaking, and runup. II: 2D. *J. of Waterway, Port,  
274 Coastal, and Ocean Engineering* 126, 48–56.
- 275 Demirbilek, Z., Webster, W.C., 1992. Application of the Green-Naghdi theory of fluid sheets  
276 to shallow-water waves, Report 1, Model formulation. US Army Wat. Exp. Sta., Coastal  
277 Engng. Res. Cntr., Vicksburg, Technical Report No. CERC-92-11 .
- 278 Engsig-Karup, A.P., Hesthaven, J.S., Bingham, H.B., Warburton, T., 2008. DG-FEM so-  
279 lution for nonlinear wave-structure interaction using Boussinesq-type equations. *Coastal  
280 Engineering* 55, 197–208.
- 281 Ertekin, R.C., Hayatdavoodi, M., Kim, J.W., 2014. On some solitary and cnoidal wave  
282 diffraction solutions of the Green–Naghdi equations. *Applied Ocean Research* 47, 125–137.

283 Ertekin, R.C., Sundararaghavan, H., 2003. Refraction and diffraction of nonlinear waves  
284 in coastal waters by the Level I Green-Naghdi equations, in: Proc. 22nd Int. Conf. on  
285 Offshore Mechanics and Arctic Engineering (OMAE 2003), June 8-13, Cancun, Mexico.

286 Ertekin, R.C., Webster, W.C., Wehausen, J.V., 1986. Waves caused by a moving disturbance  
287 in a shallow channel of finite width. *J. Fluid Mechanics* 169, 275–92.

288 Eskilsson, C., Sherwin, S.J., 2006. Spectral/hp discontinuous Galerkin methods for modelling  
289 2D Boussinesq equations. *J. of Computational Physics* 212, 566–589.

290 Green, A.E., Laws, N., Naghdi, P.M., 1974. On the theory of water waves. *Proc. Roy. Soc.*  
291 *of London. A. Mathematical and Physical Sciences* 338, 43–55.

292 Green, A.E., Naghdi, P.M., 1976. Directed fluid sheets. *Proc. Roy. Soc. of London. A.*  
293 *Mathematical and Physical Sciences* 347, 447–473.

294 Hayatdavoodi, M., Neill, D.R., Ertekin, R.C., 2018. Diffraction of cnoidal waves by vertical  
295 cylinders in shallow water. *Theoretical and Computational Fluid Dynamics* 32,8, 561–591.

296 Kennedy, A.B., Fenton, J.D., 1996. A fully nonlinear 3D method for the computation of  
297 wave propagation. *Coastal Engineering Proceedings* 1, 1102–1115.

298 Kim, J.W., Bai, K.J., Ertekin, R.C., Webster, W.C., 2001. A derivation of the Green-Naghdi  
299 equations for irrotational flows. *J. Engineering Mathematics* 40, 17–42.

300 Kim, J.W., Bai, K.J., Ertekin, R.C., Webster, W.C., 2003. A strongly-nonlinear model for  
301 water waves in water of variable depth—the Irrotational Green-Naghdi model. *J. Offshore*  
302 *Mechanics and Arctic Engineering* 125, 25–32.

303 Kim, J.W., Ertekin, R.C., Bai, K.J., 2010. Linear and nonlinear wave models based on  
304 Hamilton’s principle and stream-function theory: CMSE and IGN. *J. Offshore Mechanics*  
305 *and Arctic Engineering* 132, 021102.

306 Li, B., Fleming, C.A., 1997. A three dimensional multigrid model for fully nonlinear water  
307 waves. *Coastal Engineering* 30, 235–258.

308 Neill, D.R., Ertekin, R.C., 1997. Diffraction of solitary waves by a vertical cylinder: Green-  
309 Naghdi and Boussinesq equations, in: Proc. 16th Int. Conf. on Offshore Mechanics and  
310 Arctic Engineering, OMAE '97, January, Yokohama, Japan, pp. 63–71.

311 Neill, D.R., Hayatdavoodi, M., Ertekin, R.C., 2018. On solitary wave diffraction by multiple,  
312 in-line vertical cylinders. *Nonlinear Dynamics* 91,2, 975–994.

313 Rygg, O.B., 1988. Nonlinear refraction-diffraction of surface waves in intermediate and  
314 shallow water. *Coastal Engineering* 12, 191–211.

315 Wei, G., Kirby, J.T., 1995. Time-dependent numerical code for extended Boussinesq equa-  
316 tions. *J. Waterway, Port, Coastal, and Ocean Engineering* 121, 251–261.

317 Whalin, R., 1971. The limit of applicability of linear wave refraction theory in a convergence  
318 zone. Res. Rep. H-71-3. U. S. Army Corps of Engrs. Waterways Expt. Station, Vicksburg  
319 .

320 Wiegel, R.L., 1964. *Oceanographical Engineering*. Prentice-Hall International Englewood  
321 Cliffs, NJ.

322 Young, C.C., Wu, C.H., Liu, W.C., Kuo, J.T., 2009. A higher-order non-hydrostatic  $\sigma$  model  
323 for simulating non-linear refraction–diffraction of water waves. *Coastal Engineering* 56,  
324 919–930.

325 Zhao, B.B., Duan, W.Y., Ertekin, R.C., 2014. Application of higher-level GN theory to some  
326 wave transformation problems. *Coastal Engineering* 83, 177–189.

327 Zhao, B.B., Duan, W.Y., Ertekin, R.C., Hayatdavoodi, M., 2015a. High-level Green–Naghdi  
328 wave models for nonlinear wave transformation in three dimensions. *J. of Ocean Engineer-  
329 ing and Marine Energy* 1, 121–132.

330 Zhao, B.B., Ertekin, R.C., Duan, W.Y., 2015b. A comparative study of diffraction of shallow-  
331 water waves by high-level IGN and GN equations. *J. of Computational Physics* 283, 129–  
332 147.

333 Zhao, B.B., Duan, W.Y., Demirbilek, Z., Ertekin, R.C., Webster, W.C., 2016. A comparative  
334 study between the IGN-2 equations and the fully nonlinear, weakly dispersive Boussinesq  
335 equations. Coastal Engineering, 111, 60–69.

Author Accepted Manuscript  
Not Copied by the Journal.